BBA - Molecular Basis of Disease 1865 (2019) 2368–2378

Contents lists available at ScienceDirect

BBA - Molecular Basis of Disease

journal homepage: www.elsevier.com/locate/bbadis

CD74 knockout attenuates alcohol intake-induced cardiac dysfunction through AMPK-Skp2-mediated regulation of autophagy

Lifang Yang[a,c,*,1], Shuyi Wang[c,f,1], Jipeng Ma[b,c,1], Ji Li[d], Jian Yang[b,c], Richard Bucala[e], Jun Ren[c,f,**]

[a] Department of Anesthesiology, Xi'an Children Hospital, Xi'an 710003, China
[b] Department of Cardiovascular Surgery, Xijing Hospital, The Air Force Military Medical University, Xi'an 710032, China
[c] Center for Cardiovascular Research and Alternative Medicine, University of Wyoming, Laramie, WY 82071, USA
[d] Department of Physiology and Biophysics, Mississippi Center for Heart Research, University of Mississippi Medical Center, Jackson, MS 39216, USA
[e] Department of Medicine, Yale School of Medicine, New Haven, CT 06520, USA
[f] Shanghai Institute of Cardiovascular Diseases, Zhongshan Hospital, Fudan University, Shanghai 200032, China

ARTICLE INFO

Keywords:
CD74
Ethanol
Cardiomyocyte
Autophagy
AMPK
Skp2

ABSTRACT

CD74, a non-polymorphic type II transmembrane glycoprotein and MHC class II chaperone, is the cell surface receptor for the inflammatory cytokine macrophage migration inhibitory factor (MIF) and participates in inflammatory signaling regulation. This study examined the potential role of CD74 in binge drinking-induced cardiac contractile dysfunction. WT and CD74 knockout mice were exposed to ethanol (3 g/kg/d, i.p., for 3 days). Echocardiography, cardiomyocyte function, histological staining and autophagy signaling including AMPK, mTOR, and AMPK downstream signals Skp2 and Sirt1 were evaluated. Our results revealed that ethanol challenge overtly compromised echocardiographic, cardiomyocyte contractile, intracellular Ca^{2+} and ultrastructural properties along with overt apoptosis, inflammation (elevated MIF, IL-1β and IL-6) and mitochondrial O_2^- production ($p < 0.01$), the effect of which was reconciled by CD74 ablation ($p < 0.01$ *vs.* ethanol group) with the exception of MIF expression. Ethanol challenge upregulated autophagy ($p < 0.001$), promoted AMPK phosphorylation and Sirt1 levels ($p < 0.003$) while suppressing mTOR phosphorylation and Skp2 levels ($p < 0.02$). These effects were reversed by CD74 ablation. *In vitro* studies demonstrated that short-term ethanol challenge compromised cardiomyocyte contractile function and facilitated GFP-Puncta formation, which were mitigated by CD74 knockout ($p < 0.0001$). Moreover, the CD74 ablation-offered beneficial effects against ethanol-induced cardiomyocyte dysfunction, and GFP-Puncta formation were nullified by the AMPK activator AICAR, the Skp2 inhibitor C1 or the Sirt1 activator SRT1720 ($p < 0.0001$). Taken together, our data revealed that CD74 ablation counteracts acute ethanol challenge-induced myocardial dysfunction, inflammation and apoptosis possibly through an AMPK-mTOR-Skp2-mediated regulation of autophagy.

1. Introduction

Although low to moderate consumption of alcohol (ethanol) benefits cardiovascular function and lowers overall cardiovascular morbidity and mortality [1–3], binge drinking may severely compromise myocardial architecture and cardiac pump contractile capacity [4–7] leading to the condition of alcoholic cardiomyopathy with frequent alcohol binge intake [3,8–10]. Several cellular and molecular mechanisms have been postulated for acute cardiac toxicity of ethanol including direct effects from ethanol or its metabolic products such as

Abbreviations: AICAR, 5′-aminoimidasole-4-carboxamide-1-β-d-ribofuranoside; AMPK, 5′ adenosine monophosphate-activated protein kinase; DHE, dihydroethidium; − dL/dt, maximal velocity of relengthening; + dL/dt, maximal velocity of shortening; EDD, end diastolic dimension; ESD, end systolic dimension; ΔFFI, fura-fluorescence intensity change; GFP, green fluorescence Protein; IL, interleukin; LV, left ventricle; MIF, migration inhibitory factor; mTOR, mechanistic target of rapamycin; NCM, *Neonatal cardiomyocyte*; PS, peak shortening; Sirt, sirtuin; Skp2, S-phase kinase-associated protein 2; TEM, Transmission electron microscopy; TPS, time-to-peak shortening; TR_{90}, time-to-90% relengthening; WT, Wild type

* Correspondence to: L. Yang, Department of Anesthesiology, Xi'an Children Hospital, Xi'an 710003, China.
** Correspondence to: J. Ren, University of Wyoming College of Health Sciences, Laramie, WY 82071, USA.
E-mail addresses: yanglf@fmmu.edu.cn (L. Yang), jren@uwyo.edu (J. Ren).
[1] Equal contribution.

https://doi.org/10.1016/j.bbadis.2019.05.020
Received 24 April 2019; Received in revised form 22 May 2019; Accepted 30 May 2019
Available online 02 June 2019
0925-4439/

acetaldehyde, oxidative stress and mitochondrial damage, and various forms of cell death [*e.g.*, necrosis, apoptosis and autophagic cell death (autosis)] [2,3,11–14]. Nonetheless, the precise mechanisms responsible for binge drinking-induced cardiovascular anomalies remain poorly understood, imposing a major threat for the proper management of cardiac health in populations with frequent binge drinking.

Earlier evidence has supported an important role for macrophage migration inhibitory factor (MIF), a pluripotent cytokine constitutively expressed and stored in various cell types including immune, endothelial, and epithelial cells, in alcohol-induced liver injury [15,16]. MIF exacerbates ethanol-induced liver injury through promoting chemokine production and immune cell infiltration *via* interaction with its receptor CD74 [15,17]. Paradoxically, results from our own group have recently depicted a beneficial role for MIF in obesity and pressure overload-induced cardiac anomalies through regulation of autophagy, a highly conserved machinery to removed long-lived or damaged proteins or cell components [18,19]. However, the role of the MIF or its membrane receptor CD74 in ethanol-induced cardiotoxicity remains unknown. To this end, the current study was designed to examine the impact of genetic CD74 deficiency on acute ethanol challenge-induced cardiac geometric and functional anomalies as well as the underlying mechanisms involved. Cardiac geometry, ultrastructure and contractile function were scrutinized in WT and CD74 knockout mice with or without binge ethanol challenge. Given that our earlier findings demonstrated an important role for hyperactivation of adenosine monophosphate-activated protein kinase (AMPK) and AMPK-associated autophagy in the pathogenesis of alcoholic cardiomyopathy [13,20–22], autophagy indices and AMPK-mediated autophagy regulation were monitored. Recent evidence revealed an essential role for S-phase kinase-associated protein 2 (Skp2), a F-box component of Skp1/Cullin/F-box protein-type ubiquitin ligase, in ubiquitination and proteasomal degradation downstream of AMPK signaling [23]. We went on to examine the possible role for Skp2 in ethanol toxicity-induced responses in cardiac contractile function and autophagy. Levels of Skp2 are elevated in multiple pathological conditions such as cancer [24] although little is known for alcoholic diseases.

2. Materials and methods

2.1. Experimental animals and acute ethanol treatment

All animal procedures were approved the University of Wyoming Institute of Animal Care and Use Committee (Laramie, WY, USA) and Zhongshan Hospital Fudan University (Shanghai, China) in accordance with the NIH Guide for the Care and Use of Laboratory Animals. In brief, 5–6 month-old adult male C57BL/6 WT and CD74 knockout ($Cd74^{-/-}$) mice were injected intraperitoneally with ethanol (3 g/kg/d, twice a day at 10:00 and 20:00 h) for 3 consecutive days to mimic binge ethanol exposure defined in our laboratory and others [13,22,25–27]. Mice from non-ethanol group received an equal volume of saline. Production of $Cd74^{-/-}$ mice were described in detail previously [28]. All experimental mice were housed in a temperature-controlled room under a 12 hr/12 hr-light/dark and were allowed access to water *ad libitum*. Mice were sacrificed under anesthesia (80 mg/kg ketamine and 12 mg/kg xylazine, i.p.) 24 h after last ethanol injection, blood samples were collected and were immediately deproteinized with 6.25% trichloroacetic acid solution. Hearts were collected in liquid nitrogen. Blood ethanol levels were determined using an Alcohol/Ethanol Assay kit from (Cell Biolab, Inc., San Diego, CA).

2.2. Echocardiographic assessment

Cardiac geometry and function were evaluated in anesthetized (ketamine 80 mg/kg and xylazine 12 mg/kg, i.p.) mice 24 h after the last ethanol challenge using a 2-dimensional (2-D) guided M-mode echocardiography (Vevo 2100, FUJIFILM Visualsonics, Toronto, ON, Canada) equipped with a 22–55 MHz linear transducer (MS550D, FUJIFILM VisualSonics, Toronto, ON, Canada). Hearts were imaged in the 2-D mode using the parasternal long-axis view before switching to M-mode positioned perpendicular to interventricular septum and posterior wall of left ventricle (LV). Diastolic LV wall thickness, LV end diastolic dimension (EDD) and LV end systolic dimension (ESD) were measured. Fractional shortening was calculated as [(EDD-ESD)/EDD] × 100. Heart rate was averaged over 10 cardiac cycles [29].

2.3. Isolation of cardiomyocytes and measurement of mechanical properties

Immediately following echocardiographic evaluation, hearts were removed under anesthesia (ketamine 80 mg/kg and xylazine 12 mg/kg, i.p.) and were digested by Liberase Blendzyme (Roche). Only rod-shaped cardiomyocytes with clear edges were used. Cardiomyocytes were visualized with an inverted microscope (IX-70, Olympus, Tokyo, Japan) and mechanical properties of cardiomyocytes were evaluated using a SoftEdge MyoCam system (IonOptix Corporation, Milton, MA, USA) [30]. Peak shortening, time-to -peak shortening (TPS), time-to-90% relengthening (TR_{90}), and maximal velocity of shortening and relengthening (± dL/dt) were assessed. To evaluate the role of AMPK, Skp2 and Sirt1 in ethanol-induced responses, cardiomyocytes from adult WT or $Cd74^{-/-}$ mice were incubated with ethanol (240 mg/dl) at 37 °C for 6 h in the absence or presence of the AMPK activator 5′-aminoimidasole-4-carboxamide-1-β-d-ribofuranoside (AICAR, 500 μM) [31], or the Skp2 inhibitor C1 (10 μM) [32], or the Sirt1 activator SRT1720 (1 μM) [33] prior to assessment of mechanical properties.

2.4. Intracellular Ca^{2+} transients

Cardiomyocytes were incubated with fura-2/AM (0.5 μM; Molecular Probes) for 10 min and fluorescence intensity was recorded with a dual-excitation fluorescence photomultiplier system (IonOptix). Myocytes were placed onto an Olympus IX-70 inverted microscope and imaged through a Fluor× 40 oil objective. Cells were exposed to light emitted by a 75-W lamp and passed through either a 360- or a 380-nm filter, while being stimulated to contract at 0.5 Hz. Fluorescence emissions were detected between 480 and 520 nm and qualitative change in fura-2 fluorescence intensity (FFI) was inferred from the FFI ratio at the two wavelengths (360/380). Fluorescence decay time was calculated as an indicator of intracellular Ca^{2+} clearing [31].

2.5. Histological staining

After anesthesia, hearts were excised and immediately placed in 10% neutral-buffered formalin at room temperature for 48 h after a brief wash with PBS. The specimen were embedded in paraffin and then cut into 3-μm sections. The normal procedure of hematoxylin and eosin staining (H&E staining) were applied to examine the histological changes following ethanol treatment. The sections were examined and the images were obtained under a microscope (DXM1200F, Nikon) [31].

2.6. Transmission electron microscopy (TEM)

Myocardial ultrastructure was evaluated using TEM. In brief, hearts were fixed with PIPES-buffered formaldehyde-glutaraldehyde. Left ventricular myocardium was taken from the midventricular region and was trimmed to 1-mm^3 blocks. The blocks were fixed using a 10:1 fluid/tissue ratio overnight at 4 °C. After washing with PIPES buffer along with 2% sucrose (pH 7.4), myocardial blocks were further processed in PIPES buffered 1% OsO_4 along with 2% sucrose and 1.5% $K_3FE(CN)_6{\cdot}3H_2O$ overnight at 22–24 °C. Blocks were then dehydrated using graded ethanol and propylene oxide, and were ultimately enclosed in Epon/Araldite. RMC-MTXL ultramicrotome and a Diatome diamond knife were used to obtain thin sections. Sections were labeled with lead

citrate and uranyl acetate. Micrographic pictures were taken using a Hitachi 7500 transmission electron microscope [34].

2.7. Intracellular fluorescence measurement of superoxide (O_2^-)

Intracellular O_2^- was monitored by changes in fluorescence intensity from intracellular probe oxidation. In brief, cardiomyocytes were loaded with 5 μM dihydroethidium (DHE) (Molecular Probes, Eugene, OR, USA) for 30 min at 37 °C and washed with PBS buffer. Cells were sampled randomly using an Olympus BX-51 microscope equipped with Olympus MagnaFire™ SP digital camera and ImagePro image analysis software (Media Cybernetics, Silver Spring, MD, USA). Fluorescence was calibrated with InSpeck microspheres (Molecular Probes). The fluorescence intensity values from different fields of view were calculated using the Image *J* software, and the average values are represented [35].

2.8. Western blot

Cardiac tissues from left ventricular were homogenized and subsequent sonicated in a RIPA lysis buffer with 1% protease inhibitor cocktail. Protein concentration was measured using Bradford assay. Approximately 20 μg–30 μg proteins were loaded and separated by 15% SDS-PAGE. Proteins were electrophoretically transferred to nitrocellulose membranes. The membranes were incubated in 5% non-fat milk in Tris-buffered saline buffer. After blocking, the membranes were incubated overnight at 4 °C with anti-MIF (1:1000), anti-CD74 (1:1000), anti-IL-1β (1:1000), anti-IL-6 (1:1000), anti-Bax (1:1000), anti-Bcl-2 (1:1000), anti-Caspase-3 (1:1000), anti-Atg5 (1:1000), anti-LC3B (1:500), anti-Beclin-1 (1:1000), anti-p62 (1:1000), anti-AMPK (1:1000), anti-p-AMPK (Thr^{172}, 1:500), anti-mTOR (1:1000), anti-p-mTOR (Ser^{2448}, 1:1000), anti-Skp2 (1:1000) and anti-Sirt1 (1:1000) antibodies. Membranes were incubated with horseradish peroxidase-conjugated secondary antibody (1:5000) prior to densitometry using ChemiDoc Image device (Bio-rad). GAPDH was used as loading control [34].

2.9. Neonatal cardiomyocyte (NCM) isolation and siRNA silencing

Neonatal (1–2 day-old) WT and *Cd74*$^{-/-}$ (homozygous, no genotyping needed) mice were sterilized with ethanol. Hearts were rinsed with PBS 3 times and were cut into small pieces prior to 4–5 rounds of digestion using 0.25% trypsin (Carolina, Burlington, NC, USA). For each round, 2–4 mL of trypsin was added and heart tissues were incubated at 37 °C for 10 min. The supernatant was filtered with a 200-μm cell strainer (Biologix, Lenexa, KS, USA) and neutralized in DMEM medium containing fetal bovine serum (20%), 1% penicillin and streptomycin (Gibco, Grand Island, NY, USA) to stop digestion. Tissue fragments were subjected to another round of digestion until they defragmented. Cells were centrifuged at 800 ×*g* for 10 min at room temperature and cell pellets were resuspended in DMEM medium containing fetal bovine serum (20%) with 1% penicillin and streptomycin before being plated in an uncoated dish for 1 h at 37 °C. The suspending cardiomyocytes were plated in a confocal plate pre-coated with 1% gelatin, and cultured for 48 h at 37 °C in the presence of 95% O_2 and 5% CO_2 [34]. Cells were transfected with Skp2 siRNA (F: 5′-CCACAUGGACUGCUCUCAATT-3′; and R: 5′- UUGAGAGCAGUCCAUG UGGTT-3′) in DMEM. Forty-eight hrs later, neonatal cardiomyocytes were exposed to ethanol (240 mg/dl) for another 24 h prior to biochemical assessment.

2.10. LC3B-GFP-adenoviral transfection and drug treatment

NCM from 1 to 2 day-old WT and *Cd74*$^{-/-}$ mice were transfected with GFP-LC3 adenovirus for 24 h [34] and were treated ethanol (240 mg/dl) at 37 °C for 24 h in the absence or presence of the AMPK activator AICAR (500 μM) [31], or the Skp2 inhibitor C1 (10 μM) [32], or the Sirt1 activator SRT1720 (1 μM) [33]. After treatment, cells were gently rinsed with PBS 3 times before being fixed in 4% paraformaldehyde (20 min at room temperature). Cells were rinsed with PBS after fixation. For autophagy visualization, cells were imaged using the EVOS® FL Imaging System at ×20 magnification (Life Technologies, Carlsbad, CA, USA) and number of GFP-LC3 puncta per cell were counted.

2.11. Statistical analysis

Data are expressed as the mean ± SEM. Statistical significance ($p < 0.05$) for each variable was estimated by analysis of variance followed by Tukey's test for *post hoc* analysis.

3. Results

3.1. Echocardiographic characteristics of WT and CD74 knockout mice exposed to ethanol

Neither acute ethanol challenge nor CD74 ablation overtly affected body and organ (heart, liver and kidney) weights (or organ size when normalized to body weight) ($p > 0.05$ *vs.* WT group). Acute ethanol challenge significantly increased blood ethanol levels ($p < 0.05$ *vs.* non-treated groups) in a comparable manner in both WT and *Cd74*$^{-/-}$ mice. Acute ethanol challenge increased LVESD and decreased fractional shortening ($p < 0.01$) without affecting LVEDD and diastolic LV wall thickness, the effect of which was negated by CD74 ablation

Table 1
Biometric and myocardial contractile parameters of alcohol-treated WT and *Cd74*$^{-/-}$ mice.

Parameter	WT	*Cd74*$^{-/-}$	WT-ETOH	*Cd74*$^{-/-}$-ETOH
Body weight (g)	26.6 ± 0.7	25.5 ± 0.6	25.5 ± 0.8	26.4 ± 0.8
Heart weight (mg)	143 ± 3	140 ± 3	141 ± 4	143 ± 4
Heart/body weight (mg/g)	5.29 ± 0.09	5.51 ± 0.09	5.55 ± 0.07	5.42 ± 0.09
Liver weight (g)	1.25 ± 0.03	1.23 ± 0.02	1.25 ± 0.03	1.26 ± 0.05
Liver/body weight (mg/g)	46.8 ± 0.5	48.5 ± 0.9	49.3 ± 1.6	47.5 ± 0.8
Kidney weight (g)	0.321 ± 0.008	0.319 ± 0.011	0.312 ± 0.014	0.316 ± 0.011
Kidney/body weight (mg/g)	12.2 ± 0.3	12.5 ± 0.3	12.2 ± 0.4	12.0 ± 0.2
Blood alcohol (mg/dl)	Undetectable	Undetectable	63.3 ± 4.7*	58.4 ± 5.2*
LV wall thickness (mm)	0.88 ± 0.08	0.85 ± 0.06	0.85 ± 0.06	0.89 ± 0.06
Heart rate (bpm)	461 ± 10	454 ± 14	474 ± 16	478 ± 11
LV ESD (mm)	1.51 ± 0.14	1.39 ± 0.10	2.18 ± 0.15*	1.52 ± 0.12$^{\#}$
LV EDD (mm)	3.07 ± 0.11	2.89 ± 0.07	3.09 ± 0.20	3.01 ± 0.12
Fractional shortening (%)	52.1 ± 3.4	52.1 ± 2.4	29.8 ± 1.4*	49.4 ± 3.5$^{\#}$

LV: left ventricular; ESD: end systolic diameter; EDD: end diastolic diameter; Mean ± SEM, n = 8–9 mice per group, *$p < 0.01$ *vs.* WT group, $^{\#}p < 0.05$ *vs.* WT-ETOH group.

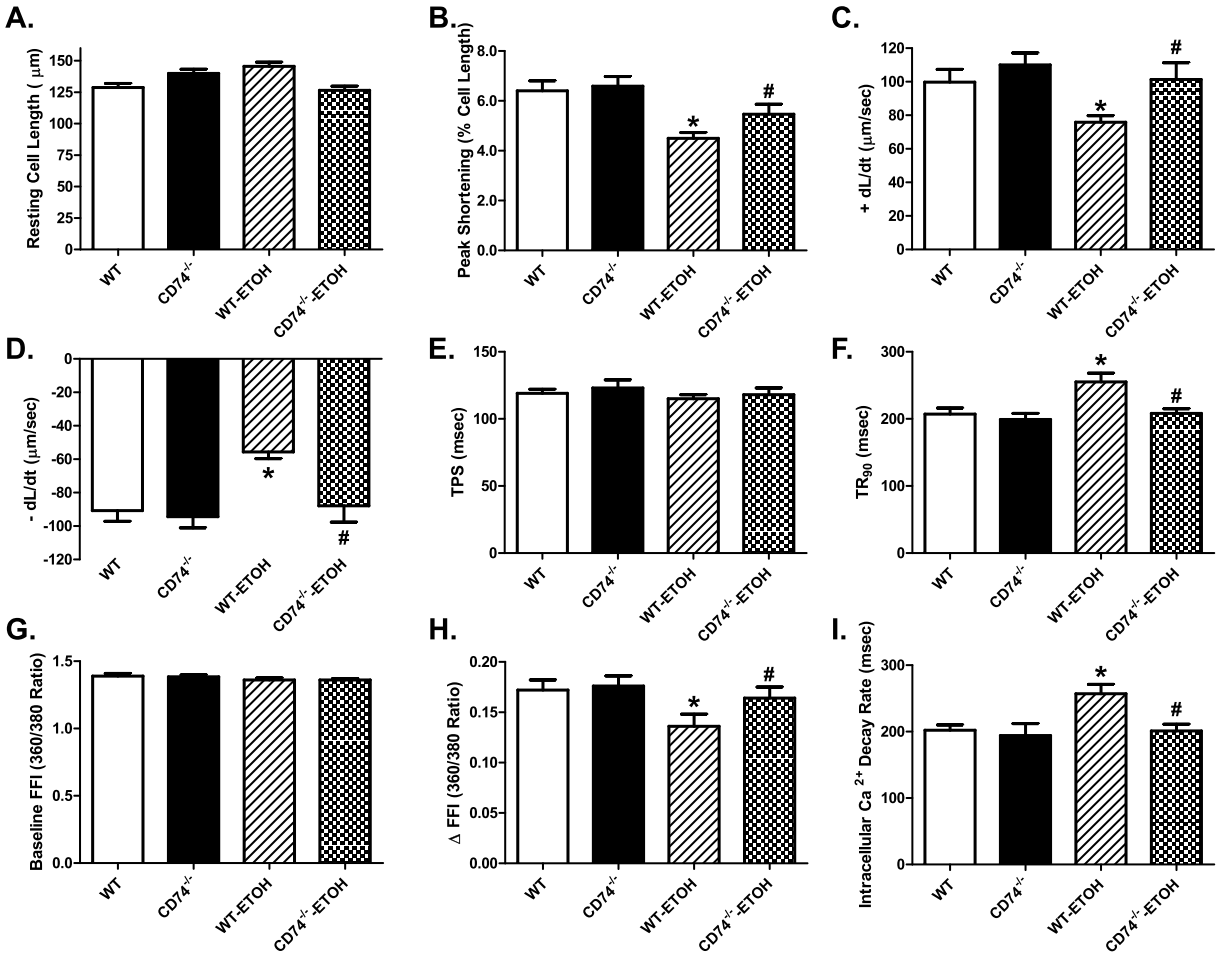

Fig. 1. Cardiomyocyte contractile and intracellular Ca^{2+} handling properties from WT and *Cd74*$^{-/-}$ mice with or without acute ethanol challenge. A: Resting cell length; B: Maximal velocity of shortening (+ dL/dt); C: Maximal velocity of relengthening (− dL/dt); D: Peak shortening (PS, normalized to resting cell length); E: Time-to-peak shortening (TPS); F: Time-to-90% relengthening (TR_{90}); G: Resting Fura-2 fluorescence intensity (FFI); H: Electrically-stimulated rise in FFI (ΔFFI); and I: Intracellular Ca^{2+} decay rate. Mean ± SEM, n = 79–80 cells (panel A–F) or 51 cells (panel G–I) from 4 mice per group, *$p < 0.05$ *vs.* WT group, $^{\#}p < 0.05$ *vs.* WT-ETOH group.

($p < 0.01$ *vs.* WT-ETOH group) with little effect from CD74 ablation itself. Neither acute ethanol challenge nor CD74 ablation affected heart rate (Table 1).

3.2. Cardiomyocyte mechanics and intracellular Ca^{2+} in WT and CD74 knockout mice

Neither ethanol challenge nor CD74 knockout altered the resting cell length. However, acute ethanol challenge significantly decreased peak shortening ($p < 0.0001$) and ± dL/dt ($p < 0.01$) associated with prolonged TR_{90} ($p = 0.0002$) without affecting TPS, the effect of which was reconciled by CD74 knockout. CD74 knockout itself did not affect cardiomyocyte mechanics (Fig. 1A–F). To explore the possible mechanisms behind CD74 ablation-induced benefit against ethanol-induced cardiac anomalies, intracellular Ca^{2+} handling was evaluated in WT and *Cd74*$^{-/-}$ cardiomyocytes with or without ethanol challenge. Our data revealed that acute ethanol challenge significantly depressed electrically-induced rise in intracellular Ca^{2+} (ΔFFI) ($p = 0.0069$) and prolonged intracellular Ca^{2+} decay ($p = 0.0023$) without affecting baseline intracellular Ca^{2+} ($p = 0.3325$), the effect of which was reversed by CD74 ablation. CD74 deletion also negated ethanol-elicited changes in ΔFFI and intracellular Ca^{2+} decay without affecting any notable alteration on intracellular Ca^{2+} properties in the absence of ethanol challenge (Fig. 1G–I).

3.3. Effect of acute ethanol exposure on myocardial histology, ultrastructure and mitochondrial O2- production in WT and CD74 knockout mice

H&E staining indicated that neither acute ethanol challenge nor CD74 ablation affected cardiomyocyte cross-section area. TEM was employed to evaluate the ultrastructure of sarcomere and mitochondria. Our data depicted overt cytoarchitectural aberration such as distortion of sarcomeres and myocardial filaments in ethanol-treated mouse myocardium, the response was negated by CD74 knockout without any notable ultrastructural change from CD74 ablation itself (Fig. 2A–B). Moreover, we evaluated mitochondrial O_2^- production. Our data revealed that ethanol challenge increased mitochondrial O_2^- production ($p < 0.0001$ *vs.* WT group), the effect of which was obliterated by CD74 knockout ($p < 0.0001$ *vs.* WT-ETOH group). CD74 knockout itself did not affect mitochondrial O_2^- production (Fig. 2C–D).

3.4. Effects of acute ethanol exposure and CD74 knockout on inflammation and apoptosis

To examine possible role of inflammation and apoptosis in CD74 ablation and acute ethanol challenge-induced contractile response, protein markers for inflammation and apoptosis including the CD74 ligand MIF, IL-1β, IL-6, Bax, Bcl-2 and Caspase-3 were assessed. Western blot results indicated that acute ethanol challenge significantly

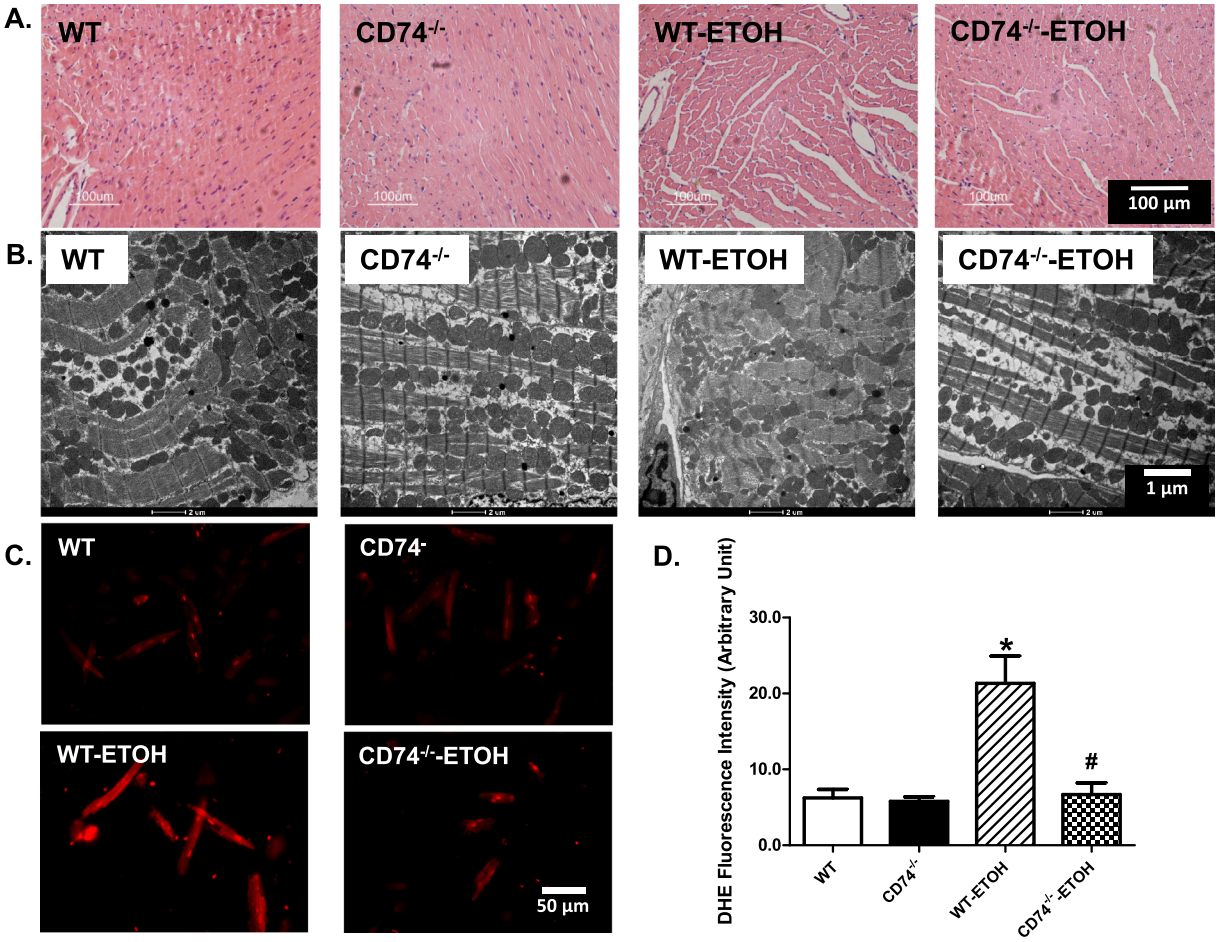

Fig. 2. Myocardial morphology, ultrastructure, mitochondrial integrity and mitochondrial O_2^- production in from WT and *Cd74*$^{-/-}$ mice with or without acute ethanol challenge. A: H&E staining (400×); B: Mitochondria and sarcomere ultrastructure using transmission electron microscopy; C: Mitochondrial superoxide (O_2^-) production using DHE staining; and D: Pooled data of mitochondrial O_2^- levels. Mean ± SEM, n = 8 images per group, *p < 0.05 *vs.* WT group; #p < 0.05 *vs.* WT-ETOH group.

upregulated the levels of MIF ($p < 0.0001$), IL-1β ($p = 0.0003$), IL-6 ($p < 0.0001$), Bax ($p < 0.0001$), Bcl-2 ($p = 0.0138$) and Caspase-3 ($p = 0.0101$) without affecting levels of CD74, the effect of which was cancelled off by CD74 ablation with the exception of MIF. CD74 knockout was validated using Western blot analysis (Fig. 3B, $p < 0.001$ between WT and *cd74*$^{-/-}$ groups). CD74 knockout alone did not change the levels of these inflammation (except for CD74) or apoptosis markers (Fig. 3).

3.5. Effects of acute ethanol exposure and CD74 knockout on autophagy

To examine possible role of autophagy in CD74 ablation and ethanol-induced contractile response, protein markers for autophagy including Atg5, LC3BI/II, and p62 were assessed. Western blot results indicated that acute ethanol challenge significantly upregulated the levels of Atg5 ($p = 0.0006$), LC3BII-to-LC3BI ratio ($p < 0.0001$) and p62 ($p = 0.001$), the effect of which was nullified by CD74 ablation. CD74 knockout alone did not affect these autophagy markers (Fig. 4).

3.6. Effects of acute ethanol exposure and CD74 knockout on AMPK, mTOR, Skp2 and Sirt1 signaling

To explore the possible regulatory mechanisms of autophagy, signaling machineries for essential autophagy regulatory components including AMPK and mTOR were monitored. Our data revealed that acute ethanol challenge significantly increased and decreased the phosphorylation of AMPK and mTOR, respectively ($p = 0.0008$ and 0.0142, respectively), without affecting pan protein expression of AMPK and mTOR. Although CD74 ablation itself did affect pan and phosphorylated AMPK and mTOR, it negated ethanol-induced AMPK phosphorylation and mTOR dephosphorylation (Fig. 5A–B). Moreover, acute ethanol challenge downregulated Skp2 ($p = 0.004$), a downstream target of AMPK-mTOR in tumorigenesis and aging [36,37] while upregulating that of Sirt1 ($p = 0.0003$), the effect of which was mitigated by CD74 ablation, with little effect from CD74 knockout itself (Fig. 5C–D). Further assessment of the potential relationship between Skp2 and Sirt1 using neonatal murine cardiomyocytes revealed that siRNA silencing of Skp2 effectively negated ethanol exposure-induced upregulation of Sirt1 ($p = 0.0273$) without eliciting any effect by itself (Supplemental Fig. 1), suggesting that Skp2 is possibly upstream role of Sirt1.

3.7. Effects of AMPK activation, Skp2 inhibition and Sirt1 activation in ethanol-induced cardiomyocyte contractile abnormalities

To explore the role of AMPK, Skp2 and Sirt1 in ethanol-induced cardiac contractile properties, isolated cardiomyocytes from WT and *Cd74*$^{-/-}$ mice were challenged with ethanol (240 mg/dl) for 6 h in the absence or presence of the AMPK activator AICAR (500 μM), the Skp2 inhibitor C1 (10 μM) or the Sirt1 activator SRT1720 (1 μM) prior to assessment of cardiomyocyte mechanics. Our results shown in Fig. 6A–F revealed that ethanol significantly decreased PS, maximal velocity of

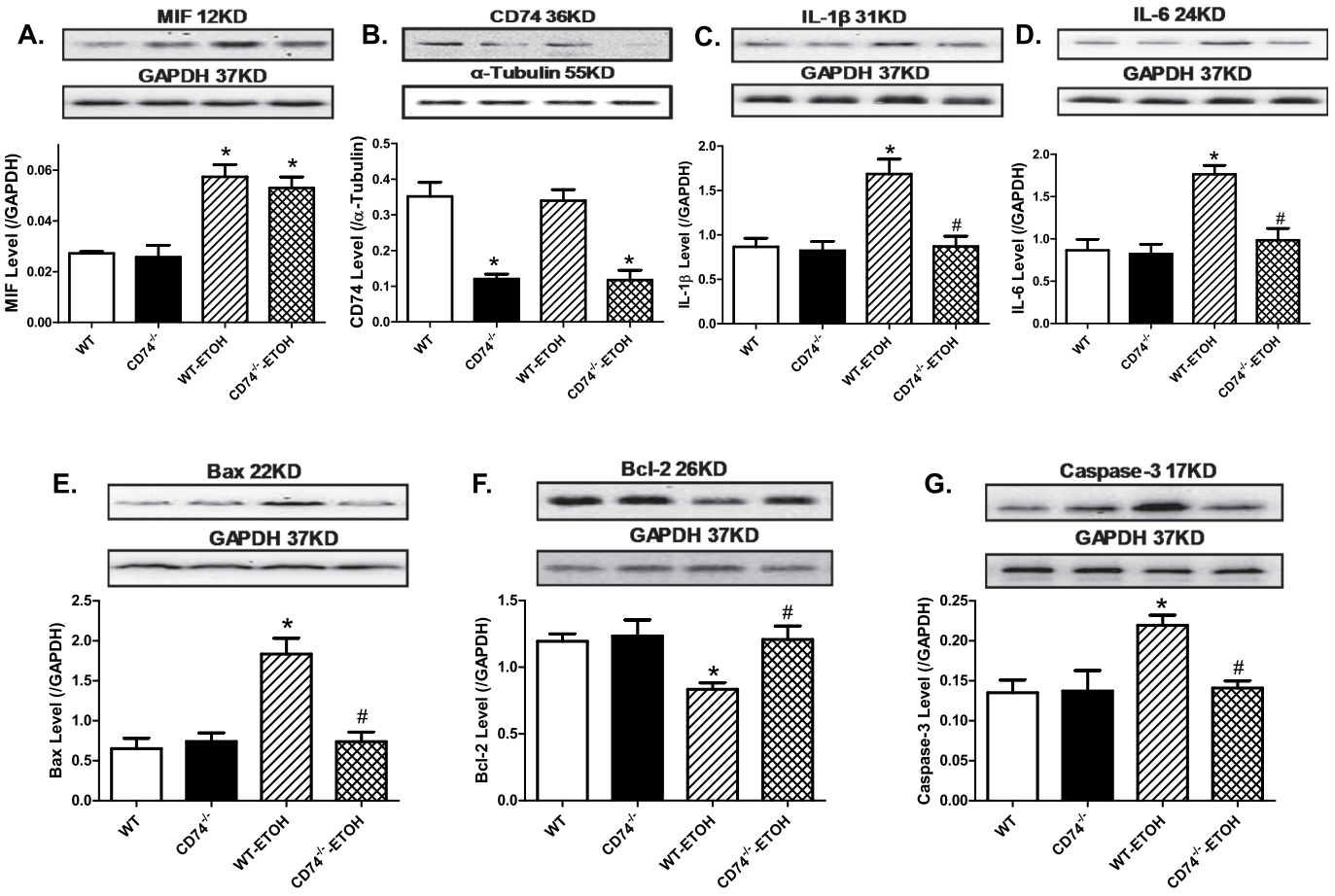

Fig. 3. Protein levels of MIF, CD74, proinflammatory and apoptotic makers in hearts from WT and *Cd74*$^{-/-}$ mice with or without acute ethanol challenge. A: MIF; B: CD74; C: IL-1β; D: IL-6; E: Bax; F: Bcl-2; and G: Caspase-3. Insets: Representative gel blots depicting levels of MIF, CD74, IL-1β, IL-6, Bax, Bcl-2 and Caspase-3 using specific antibodies (GAPDH as the loading control); Mean ± SEM, n = 5–7 mice per group, *p < 0.05 *vs.* WT group; #p < 0.05 *vs.* WT-ETOH group.

shortening/relengthening, and prolonged the duration of relengthening (p < 0.0001 *vs.* control) without affecting resting cell length and duration of shortening. Although AICAR, C1 or SRT1720 alone did not affect these mechanical properties of cardiomyocytes in the absence of short-term ethanol exposure, it nullified CD74 ablation-induced benefit against ethanol-elicited cardiomyocyte mechanical anomalies (p < 0.0001 *vs.* ETOH group). Our further assessment of the direct impact of AMPK activation on levels of Skp2 and Sirt1 revealed that incubation of AICAR (500 μM) for 6 h stimulated AMPK phosphorylation (p = 0.0014), downregulated Skp2 (p = 0.0058) and upregulated Sirt1 (p = 0.002) (Fig. 6G–I). These data consolidated a role for AMPK, Skp2 and Sirt1 in ethanol and CD74 ablation-induced cardiomyocyte contractile responses.

3.8. Effects of AMPK activation, Skp2 inhibition and Sirt1 activation in ethanol-induced GFP-LC3 formation

To discern the cause-effect relationship of AMPK, Skp2 and Sirt1 in ethanol-induced autophagic response, neonatal cardiomyocytes from WT and *Cd74*$^{-/-}$ mice were transfected with GFP-LC3 prior to exposure of ethanol (240 mg/dl) for 6 h in the absence or presence of the AMPK activator AICAR (500 μM), the Skp2 inhibitor C1 (10 μM) or the Sirt1 activator SRT1720 (1 μM). Our results indicated that ethanol overtly promoted GFP-LC3 puncta (p < 0.0001 *vs.* control group), the effect of which was mitigated by CD74 ablation. Although AICAR, C1 or SRT1720 alone did not affect GFP-LC3 puncta levels, it nullified CD74 ablation-induced benefit against ethanol-elicited GFP-LC3 puncta overproduction (p < 0.0001 *vs.* ETOH group). These data consolidated a role for AMPK, Skp2 and Sirt1 in CD74 ablation-offered protection against ethanol-induced excessive autophagosome formation (Fig. 7).

4. Discussion

The salient findings from this study demonstrate that genetic CD74 deletion protects the heart against acute ethanol exposure-elicited cardiac contractile abnormalities, mitochondrial O_2^- production, apoptosis and inflammation. In accordance with our earlier studies [22,38], acute ethanol challenge promotes autophagy, AMPK activation, mTOR dephosphorylation in association with cardiac contractile dysfunction (as depicted in Fig. 8). Our data further noted downregulation of AMPK downstream signal Skp2 and upregulation of Sirt1 in response to acute ethanol challenge. The ablation of CD74, as the MIF receptor necessary for AMPK upregulation [39], mitigated ethanol-induced cardiac dysfunction and autophagy anomalies. The *in vitro* findings suggest a permissive role for AMPK, Skp2 and Sirt1 in CD74 ablation that provides protection against acute ethanol challenge.

In this study, an acute ethanol challenge at the dose of 3 g/kg body weight was used to mimic binge drinking in humans (approximately equivalent to 90–100 g/day in human) with pronounced organ damage [40]. In particular, our results showed overt cardiac contractile dysfunction (enlarged LV ESD, compromised fractional shortening and cardiomyocyte contractile capacity), ultrastructural changes, inflammation and apoptosis without notable changes in cardiac remodeling (heart weight or size and cardiomyocyte cross-sectional area) in response to acute ethanol challenge. CD74 ablation rescued ethanol-induced functional, ultrastructural, inflammatory and apoptotic

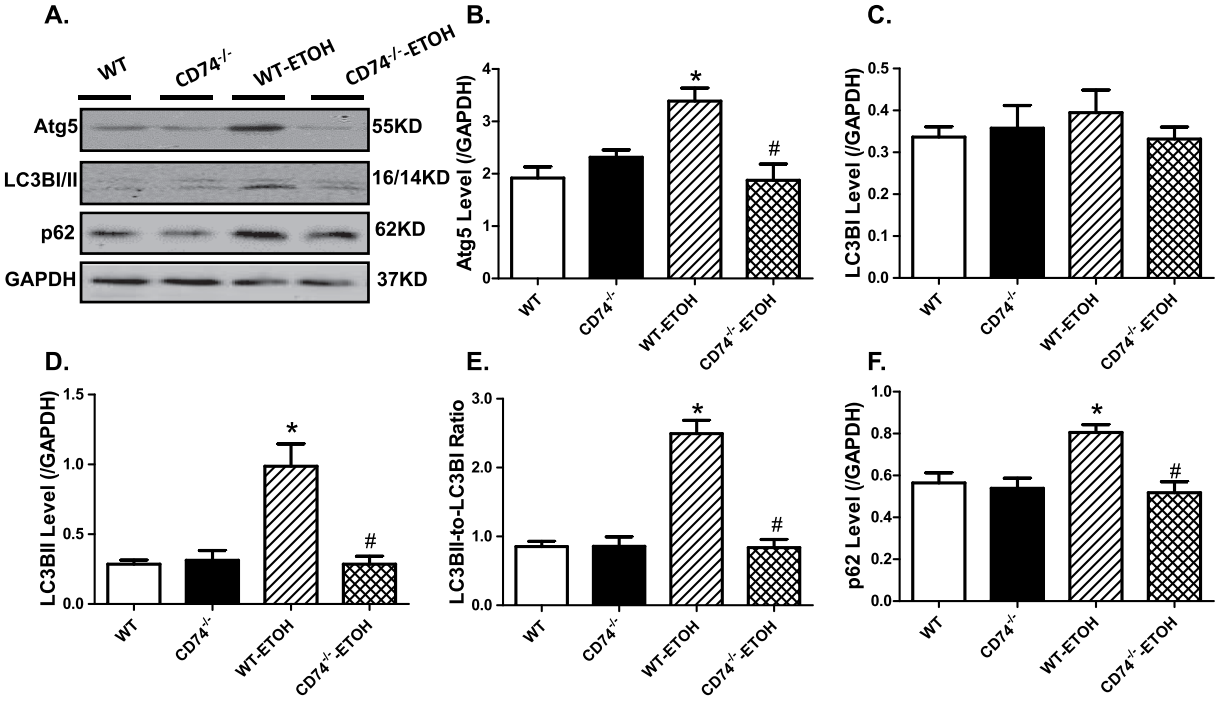

Fig. 4. Protein levels of autophagy in hearts from WT and *Cd74*$^{-/-}$ mice with or without acute ethanol challenge. A: Representative gel blots depicting levels of Atg5, LC3BI/II, and p62 using specific antibodies (GAPDH as loading control); B: Atg5; C: LC3BI; D: LC3BII; E: LC3BII-to-LC3BI ratio; and F: p62. Mean ± SEM, n = 5–7 mice per group, *p < 0.05 *vs.* WT group; #p < 0.05 *vs.* WT-ETOH group.

anomalies, supporting a key role for the MIF receptor CD74 in alcoholic cardiomyopathy. CD74 knockout mice did not show any apparent morphological or functional responses in the absence of ethanol challenge, suggesting a minimal contribution of CD74 receptor to physiological cardiac homeostasis. However with acute ethanol challenge, cardiomyocytes exhibited severely dampened intracellular Ca^{2+} release upon electrical stimulus and delayed intracellular Ca^{2+} removal, in line with our earlier findings [13,21,22]. CD74 knockout itself did not alter intracellular Ca^{2+} homeostasis although it rescued against intracellular Ca^{2+} mishandling in the face of ethanol challenge. These findings favor

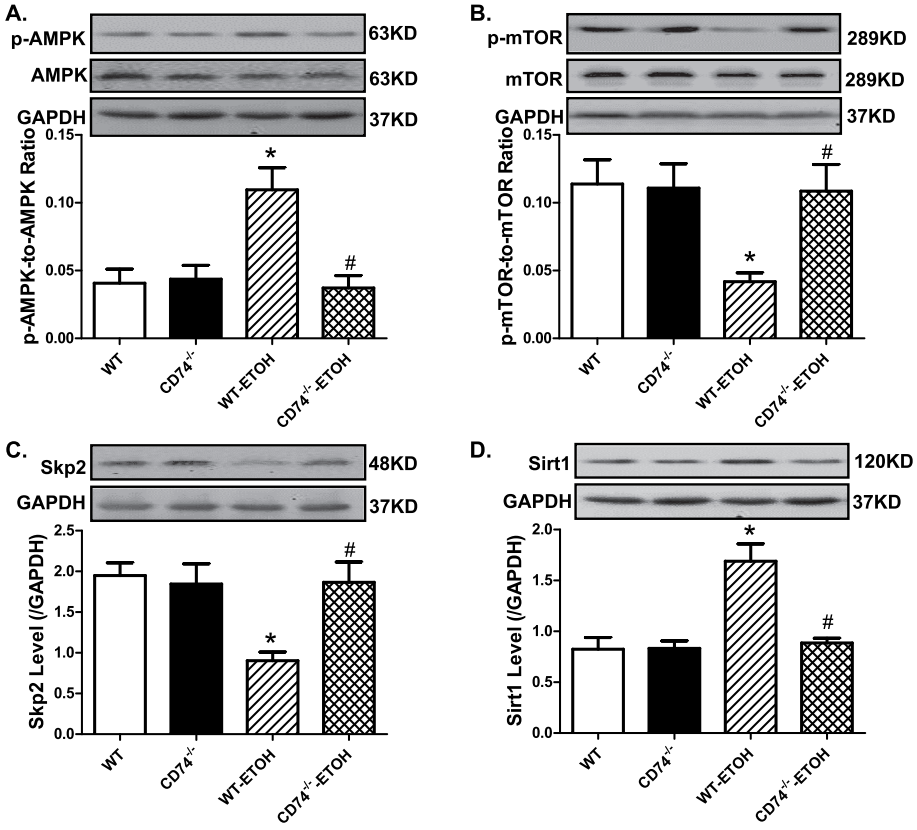

Fig. 5. Protein levels of pan and phosphorylated AMPK and mTOR, Skp2 and Sirt1 in hearts from WT and *Cd74*$^{-/-}$ mice with or without acute ethanol challenge. A: p-AMPK (Thr^{172})-to-AMPK ratio; B: p-mTOR (Ser^{2448})-to-mTOR ratio; C: Skp2; and D: Sirt1. Insets: Representative gel blots depicting levels of pan and phosphorylated AMPK and mTOR, Skp2 and Sirt1 using specific antibodies (GAPDH as loading control). Mean ± SEM, n = 5–6 mice per group, *p < 0.05 *vs.* WT group; #p < 0.05 *vs.* WT-ETOH group.

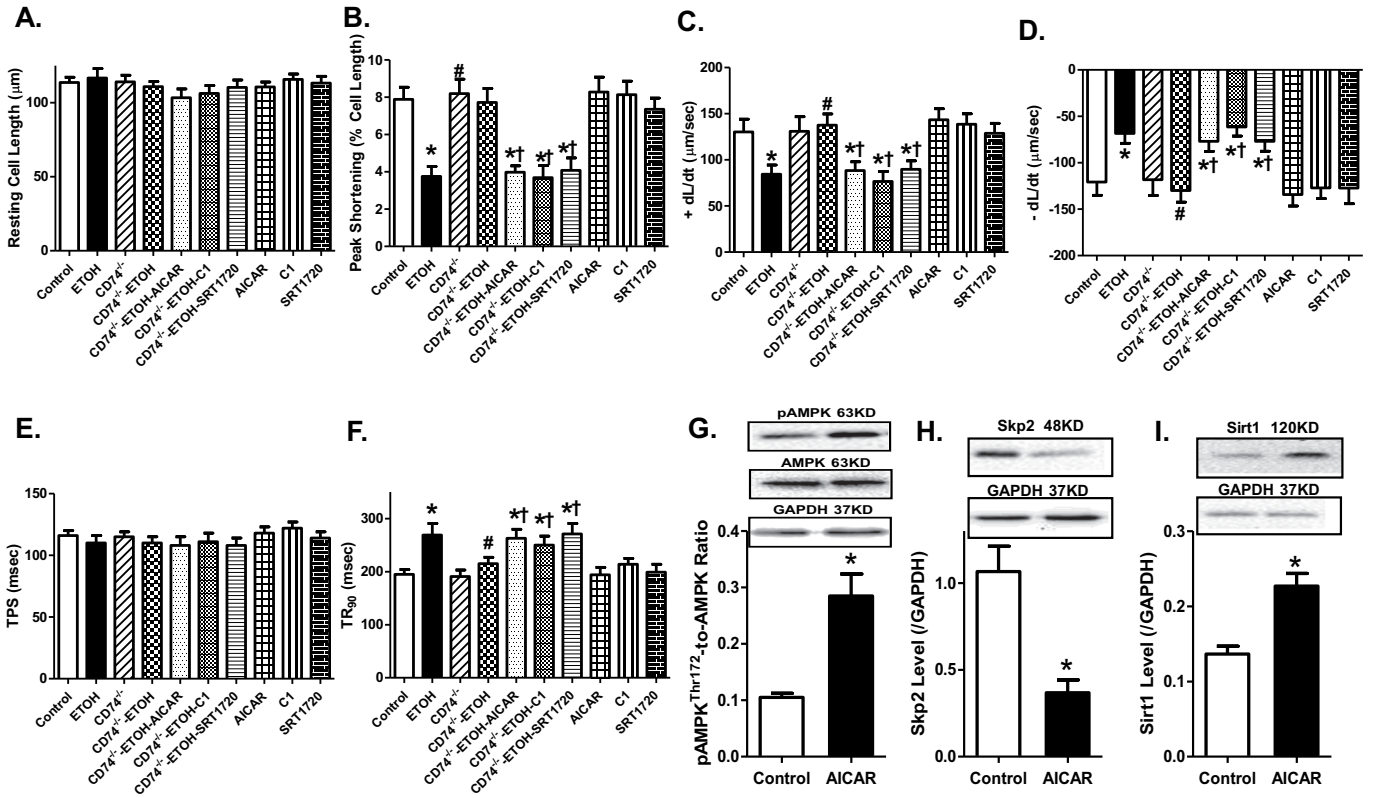

Fig. 6. Role of AMPK on Skp2 and Sirt1 levels as well as AMPK-Skp2-Sirt1 signaling in ethanol challenge-induced cardiomyocyte contractile responses. Isolated cardiomyocytes from WT or *Cd74*$^{-/-}$ mice were incubated with ethanol (240 mg/dL) for 6 h in the presence or absence of the AMPK activator AICAR (500 μM), the Skp2 inhibitor C1 (10 μM) and the Sirt1 activator SRT1720 (1 μM) prior to assessment of cardiomyocyte contractile function. To assess the direct impact of AMPK activation on levels of Skp2 and Sirt1, cardiomyocytes from WT mice were incubated with AICAR (500 μM) for 6 h before biochemical analysis. A: Resting cell length; B: Peak shortening (normalized to resting cell length; C: Maximal velocity of shortening (+ dL/dt); D: Maximal velocity of relengthening (− dL/dt); E: Time-to-peak shortening (TPS); F: Time-to-90% relengthening (TR_{90}); G: AMPK (Thr^{172}) phosphorylation; H: Skp2 levels; and I: Sirt1 levels. Mean ± SEM, n = 30 cells (panel A–F) or 5 isolations (panel H–I) per group, $^{*}p < 0.05$ *vs.* control group, $^{\#}p < 0.05$ *vs.* ethanol (ETOH) group, $^{\dagger}p < 0.05$ *vs.* CD74$^{-/-}$-ETOH.

an important role for intracellular Ca^{2+} handling in CD74 ablation with beneficial mechanical effects against acute ethanol challenge. The absence of overt cardiac remodeling in response to ethanol challenge is likely due to the short duration of alcoholism, suggesting that functional and metabolic derangement may occur sooner than discernable geometric changes in alcoholic injury [41]. In our hands, ethanol challenge failed to alter liver and kidney weights or sizes, the effect of which was unaffected by CD74 knockout. Although it is still premature to exclude any indirect effects of ethanol on the heart from other organs, the cardiac damage resulted from ethanol challenge is unlikely originated from other organs, given the short timeframe of ethanol challenge and negative findings from liver and kidney. Data from our study noted pronounced rises in cardiac MIF levels following ethanol challenge, in line with the previous findings of elevated MIF levels in alcoholism [15,16]. Not surprisingly, CD74 ablation failed to ethanol-induced elevation in MIF levels.

Data from our study revealed that CD74 knockout protects against ethanol-induced alterations in autophagy (such as protein markers of Atg5, LC3B, p62 and GFP-Puncta formation), AMPK hyperphosphorylation and mTOR dephosphorylation. Excessive autophagy has been reported in alcoholic heart damage while inhibition of autophagy using autophagy inhibitors, AMPK inhibitors or knockout preserves the heart from alcoholic damage [22,38]. Along the same line, the present findings suggest a pivotal role for autophagy regulation in CD74 knockout-offered protection against alcoholic cardiomyopathy. A number of possible mechanisms may act in CD74 ablation-induced autophagy responses. First, the AMPK-mTOR-mediated autophagy regulation may contribute to CD74 ablation-induced protection against ethanol toxicity. Ethanol challenge promotes MIF production (but not CD74 levels) and turns on AMPK [20–22], which suppresses mTOR phosphorylation and facilitates autophagy [42]. Our current findings revealed that CD74 ablation effectively suppressed AMPK activation (possibly through interrupting the MIF-AMPK signaling) [39] and restored mTOR phosphorylation in the face of acute ethanol challenge. CD74 knockout reversed ethanol-induced changes the AMPK downstream signaling molecules Skp2 and Sirt1. Along with the direct impact of AMPK activation on levels of Skp2 and Sirt1 as shown in Fig. 6, our observation favors a unique role for Skp2 and Sirt1 in acute ethanol toxicity and CD74 ablation-induced functional and autophagy responses. Recent evidence indicated an AMPK-dependent suppression of Skp2, leading to histone H3 Arg17 demethylation and autophagy induction [23]. Skp2 was shown to serve as a downstream target of AMPK-mTOR in tumorigenesis and aging [36,37]. Suppression of Skp2 using C1 effectively mitigated CD74 ablation-offered inhibition of cardiac autophagosome formation and contractile defect in response to ethanol challenge. Our data further noted that CD74 ablation suppresses AMPK-mTOR-Skp2-mediated autophagy in a Sirt1-dependent mechanism. The permissive role for Sirt1 in CD74 ablation-offered beneficial responses in autophagy and cardiac function against ethanol received consolidation from the SRT1720-induced removal of CD74 knockout-induced contractile and autophagy benefits. Although a direct link between Skp2 and Sirt1 was not provided in the current study, an inverse relationship between Skp2 and Sirtuins was noted in non-small cell lung cancers [43]. Ample evidence suggests that Skp2 functions as an oncoprotein by targeting a wide range of signaling effectors, such as the tumor suppressor p27, for degradation [44]. Our current *in vitro* findings revealed that ethanol-induced upregulation of Sirt1 protein levels may be cancelled off by silencing Skp2, suggesting a upstream

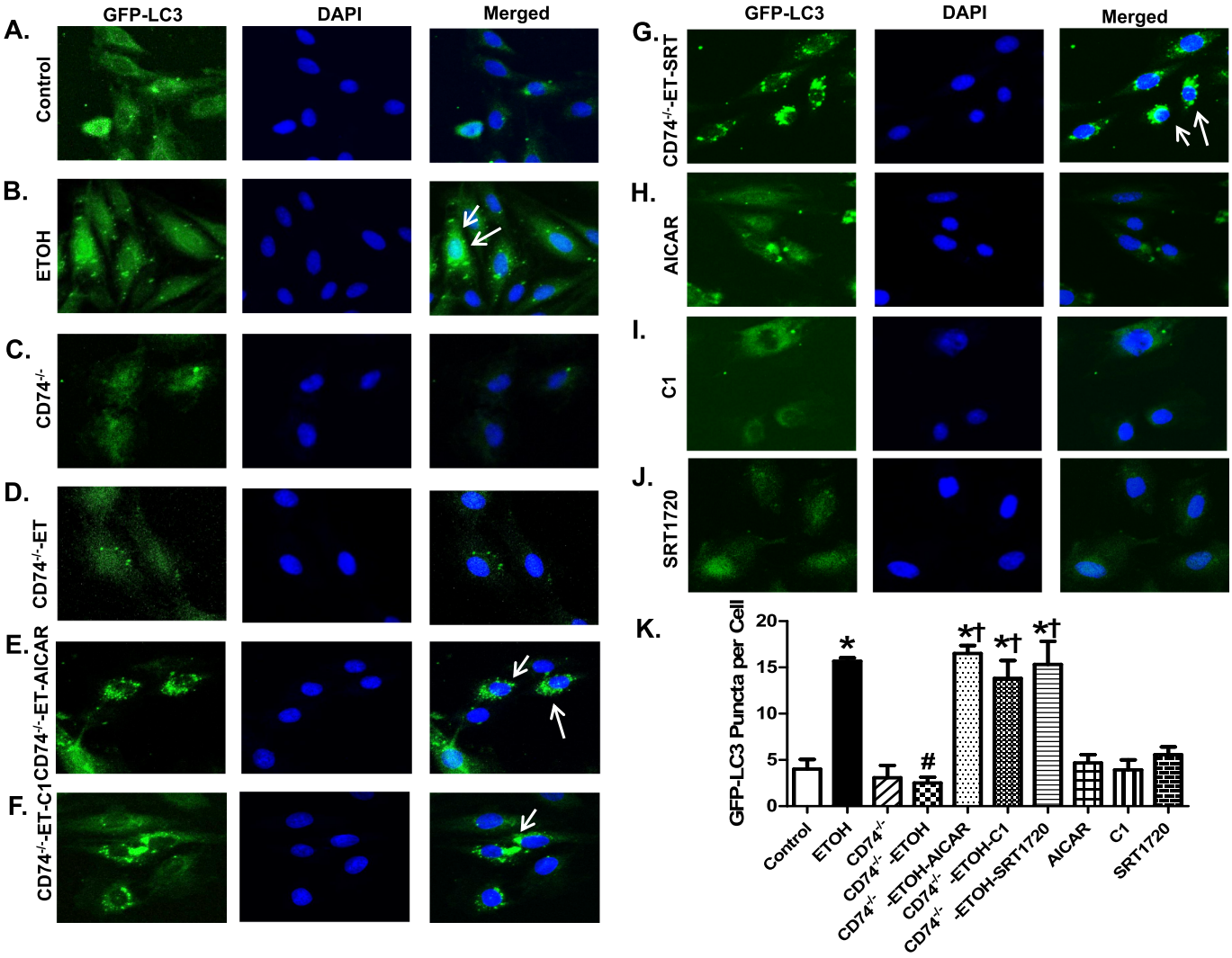

Fig. 7. Role of AMPK, Skp2 and Sirt1 in acute ethanol challenge-induced autophagy response. Neonatal cardiomyocytes from WT or *Cd74*$^{-/-}$ mice were incubated with ethanol (240 mg/dL) in the presence or absence of the AMPK activator AICAR (500 nM), the Skp2 inhibitor C1 (10 μM) and the Sirt1 activator SRT1720 (1 μM). A–J: Representative images of GFP-LC3, DAPI staining and merged images of GFP-LC3 and DAPI staining in respective neonatal cardiomyocyte group. Arrowheads denote autophagosomes; and K: Quantitative analysis of GFP-LC3 positive puncta per cell. Mean ± SEM, n = 4–5 images per group, *p < 0.05 *vs.* control group, $^{\#}$p < 0.05 *vs.* ethanol (ETOH) group, †p < 0.05 *vs.* CD74$^{-/-}$-ETOH.

role of Skp2 in the regulation of Sirt1. This was also supported by the direct regulation of AICAR on levels of Skp2 and Sirt1. Second, our results support a role for mitochondrial integrity and TEM myocardial ultrastructure in CD74 ablation-induced protection against ethanol toxicity. Our observations reveal that CD74 knockout reversed ethanol-induced changes in mitochondrial O_2^- production and TEM ultrastructure. Ethanol toxicity may perturb mitochondrial integrity, resulting in compromised morphology, oxidative stress, intracellular Ca^{2+} handling and mechanical property [2,38]. It should be noted that blood alcohol levels were around 60 mg/mL following ethanol challenge whereas 240 mg/mL was used for *in vitro* ethanol challenge. The discrepancy between *in vivo* and *in vitro* alcohol levels is mainly attributed to the presence of *in vivo* hepatic metabolism and timing of experimentation (at least 24 h after the last ethanol injection).

In conclusion, the findings from the present study indicate that CD74 participates in mediating ethanol toxicity-induced cardiac contractile and ultrastructural damage through the AMPK-mTOR-Skp2-mediated regulation of autophagy. These data collectively reveal a novel mechanism for the MIF receptor CD74 as a potential therapeutic target in the management of alcoholic organ injury possibly through regulation of autophagy.

Supplementary data to this article can be found online at https://doi.org/10.1016/j.bbadis.2019.05.020.

Transparency document

The Transparency document associated with this article can be found, in online version.

Declaration of Competing Interest

Yale University hold intellectual property rights for the therapeutic augmentation of MIF signaling in cardiac tissue protection. RB is a co-inventor on this patent and a co-founder of MIFCOR, Inc., which seeks to augment MIF pathways for ischemic tissue injury. RB receives research support from MIFCOR, Inc.

Acknowledgments

This work received supports from the National Natural Science Foundation of China (81570225, 81774415), a University of Wyoming Faculty Grant-in-Aid, and NIH (RB).

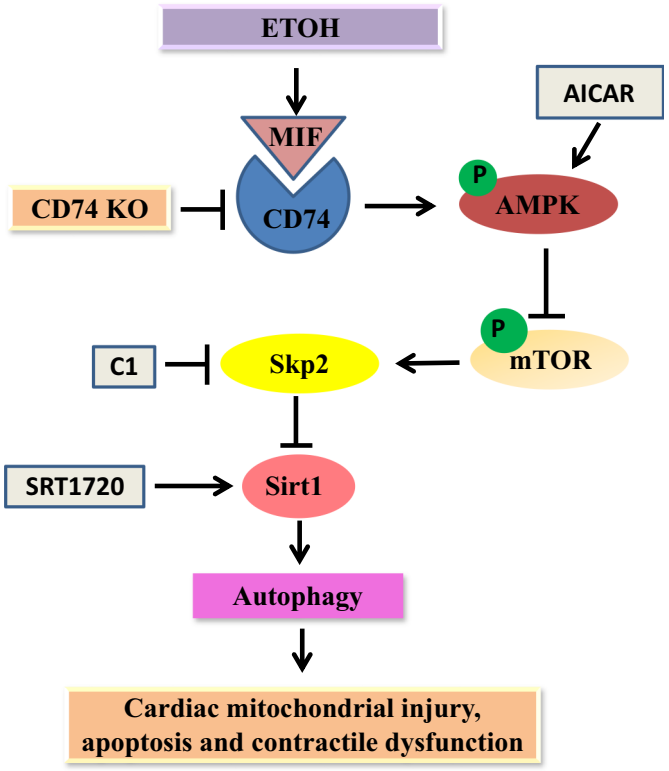

Fig. 8. Schematic diagram depicting the role of CD74, AMPK, mTOR, Skp2, and Sirt1 in acute ethanol challenge-induced changes in autophagy and cardiac function. CD74 ablation mitigates ethanol-induced AMPK phosphorylation, mTOR-dephosphorylation and inhibits autophagy through a Skp2-Sirt1-dependent mechanism. AMPK activation suppresses mTOR phosphorylation, downregulates Skp2 and upregulates Sirt1, en route to autophagy induction upon ethanol challenge. Arrowheads denote stimulation whereas "T" ending lines indicate inhibition.

Author contribution

LY, SW, JM, JR: Planned and performed the study, drafted and proved the manuscript; JY: conducted the study; JL: Edited the manuscript and discussed with the experimental design; RB: Provided *Cd74* $^{-/-}$ mice and edited the manuscript.

References

[1] T.A. Manolis, A.A. Manolis, A.S. Manolis, Cardiovascular effects of alcohol: a double-edged sword/how to remain at the nadir point of the J-curve? Alcohol 76 (2018) 117–129.
[2] Y. Zhang, J. Ren, ALDH2 in alcoholic heart diseases: molecular mechanism and clinical implications, Pharmacol. Ther. 132 (2011) 86–95.
[3] J. Fernandez-Sola, Cardiovascular risks and benefits of moderate and heavy alcohol consumption, Nat. Rev. Cardiol. 12 (2015) 576–587.
[4] E. Hookana, M.J. Junttila, V.P. Puurunen, J.T. Tikkanen, K.S. Kaikkonen, M.L. Kortelainen, R.J. Myerburg, H.V. Huikuri, Causes of nonischemic sudden cardiac death in the current era, Heart Rhythm. 8 (2011) 1570–1575.
[5] K.J. Mukamal, K.M. Conigrave, M.A. Mittleman, C.A. Camargo Jr., M.J. Stampfer, W.C. Willett, E.B. Rimm, Roles of drinking pattern and type of alcohol consumed in coronary heart disease in men, N. Engl. J. Med. 348 (2003) 109–118.
[6] R. Guo, J. Ren, Alcohol and acetaldehyde in public health: from marvel to menace, Int. J. Environ. Res. Public Health 7 (2010) 1285–1301.
[7] M.R. Piano, A. Mazzuco, M. Kang, S.A. Phillips, Cardiovascular consequences of binge drinking: an integrative review with implications for advocacy, policy, and research, Alcohol. Clin. Exp. Res. 41 (2017) 487–496.
[8] I. Laonigro, M. Correale, M. Di Biase, E. Altomare, Alcohol abuse and heart failure, Eur. J. Heart Fail. 11 (2009) 453–462.
[9] L. Djousse, J.M. Gaziano, Alcohol consumption and heart failure: a systematic review, Curr. Atheroscler. Rep. 10 (2008) 117–120.
[10] S. Wang, J. Ren, Role of autophagy and regulatory mechanisms in alcoholic cardiomyopathy, Biochim. Biophys. Acta Mol. Basis Dis. 1864 (2018) 2003–2009.
[11] V.R. Preedy, V.B. Patel, M.E. Reilly, P.J. Richardson, G. Falkous, D. Mantle, Oxidants, antioxidants and alcohol: implications for skeletal and cardiac muscle, Front. Biosci. 4 (1999) e58–e66.
[12] E.A. Laposata, L.G. Lange, Presence of nonoxidative ethanol metabolism in human organs commonly damaged by ethanol abuse, Science 231 (1986) 497–499.
[13] R. Guo, J. Ren, Alcohol dehydrogenase accentuates ethanol-induced myocardial dysfunction and mitochondrial damage in mice: role of mitochondrial death pathway, PLoS One 5 (2010) e8757.
[14] M.R. Piano, Alcohol's effects on the cardiovascular system, Alcohol Res. 38 (2017) 219–241.
[15] M.A. Barnes, M.R. McMullen, S. Roychowdhury, S.G. Pisano, X. Liu, A.B. Stavitsky, R. Bucala, L.E. Nagy, Macrophage migration inhibitory factor contributes to ethanol-induced liver injury by mediating cell injury, steatohepatitis, and steatosis, Hepatology 57 (2013) 1980–1991.
[16] V. Marin, K. Poulsen, G. Odena, M.R. McMullen, J. Altamirano, P. Sancho-Bru, C. Tiribelli, J. Caballeria, N. Rosso, R. Bataller, L.E. Nagy, Hepatocyte-derived macrophage migration inhibitory factor mediates alcohol-induced liver injury in mice and patients, J. Hepatol. 67 (2017) 1018–1025.
[17] L. Leng, C.N. Metz, Y. Fang, J. Xu, S. Donnelly, J. Baugh, T. Delohery, Y. Chen, R.A. Mitchell, R. Bucala, MIF signal transduction initiated by binding to CD74, J. Exp. Med. 197 (2003) 1467–1476.
[18] X. Xu, J. Ren, Macrophage migration inhibitory factor (MIF) knockout preserves cardiac homeostasis through alleviating Akt-mediated myocardial autophagy suppression in high-fat diet-induced obesity, Int. J. Obes. 39 (2015) 387–396.
[19] X. Xu, Y. Hua, S. Nair, R. Bucala, J. Ren, Macrophage migration inhibitory factor deletion exacerbates pressure overload-induced cardiac hypertrophy through mitigating autophagy, Hypertension 63 (2014) 490–499.
[20] M.R. Kandadi, N. Hu, J. Ren, ULK1 plays a critical role in AMPK-mediated myocardial autophagy and contractile dysfunction following acute alcohol challenge, Curr. Pharm. Des. 19 (2013) 4874–4887.
[21] R. Guo, G.I. Scott, J. Ren, Involvement of AMPK in alcohol dehydrogenase accentuated myocardial dysfunction following acute ethanol challenge in mice, PLoS One 5 (2010) e11268.
[22] R. Guo, J. Ren, Deficiency in AMPK attenuates ethanol-induced cardiac contractile dysfunction through inhibition of autophagosome formation, Cardiovasc. Res. 94 (2012) 480–491.
[23] H.J. Shin, H. Kim, S. Oh, J.G. Lee, M. Kee, H.J. Ko, M.N. Kweon, K.J. Won, S.H. Baek, AMPK-SKP2-CARM1 signalling cascade in transcriptional regulation of autophagy, Nature 534 (2016) 553–557.
[24] C. Li, L. Du, Y. Ren, X. Liu, Q. Jiao, D. Cui, M. Wen, C. Wang, G. Wei, Y. Wang, A. Ji, Q. Wang, SKP2 promotes breast cancer tumorigenesis and radiation tolerance through PDCD4 ubiquitination, J. Exp. Clin. Cancer Res. 38 (2019) 76.
[25] S.L. Chang, W. Huang, H. Han, I.K. Sariyer, Binge-like exposure to ethanol enhances morphine's anti-nociception in B6 mice, Front. Psychiatry 9 (2018) 756.
[26] B. Malinowska, D. Napiorkowska-Pawlak, R. Pawlak, W. Buczko, M. Gothert, Ifenprodil influences changes in mouse behaviour related to acute and chronic ethanol administration, Eur. J. Pharmacol. 377 (1999) 13–19.
[27] H. Ma, J. Li, F. Gao, J. Ren, Aldehyde dehydrogenase 2 ameliorates acute cardiac toxicity of ethanol: role of protein phosphatase and forkhead transcription factor, J. Am. Coll. Cardiol. 54 (2009) 2187–2196.
[28] I. Shachar, R.A. Flavell, Requirement for invariant chain in B cell maturation and function, Science 274 (1996) 106–108.
[29] S. Wang, X. Zhu, L. Xiong, J. Ren, Ablation of Akt2 prevents paraquat-induced myocardial mitochondrial injury and contractile dysfunction: role of Nrf2, Toxicol. Lett. 269 (2017) 1–14.
[30] N. Hu, X. Han, E.K. Lane, F. Gao, Y. Zhang, J. Ren, Cardiac-specific overexpression of metallothionein rescues against cigarette smoking exposure-induced myocardial contractile and mitochondrial damage, PLoS One 8 (2013) e57151.
[31] S. Wang, X. Zhu, L. Xiong, Y. Zhang, J. Ren, Toll-like receptor 4 knockout alleviates paraquat-induced cardiomyocyte contractile dysfunction through an autophagy-dependent mechanism, Toxicol. Lett. 257 (2016) 11–22.
[32] L. Wu, A.V. Grigoryan, Y. Li, B. Hao, M. Pagano, T.J. Cardozo, Specific small molecule inhibitors of Skp2-mediated p27 degradation, Chem. Biol. 19 (2012) 1515–1524.
[33] J. Ren, L. Yang, L. Zhu, X. Xu, A.F. Ceylan, W. Guo, J. Yang, Y. Zhang, Akt2 ablation prolongs life span and improves myocardial contractile function with adaptive cardiac remodeling: role of Sirt1-mediated autophagy regulation, Aging Cell 16 (2017) 976–987.
[34] S. Wang, W. Ge, C. Harns, X. Meng, Y. Zhang, J. Ren, Ablation of toll-like receptor 4 attenuates aging-induced myocardial remodeling and contractile dysfunction through NCoRI-HDAC1-mediated regulation of autophagy, J. Mol. Cell. Cardiol. 119 (2018) 40–50.
[35] Y. Zhang, S.L. Mi, N. Hu, T.A. Doser, A. Sun, J. Ge, J. Ren, Mitochondrial aldehyde dehydrogenase 2 accentuates aging-induced cardiac remodeling and contractile dysfunction: role of AMPK, Sirt1, and mitochondrial function, Free Radic. Biol. Med. 71 (2014) 208–220.
[36] H. Liu, Q. Yue, S. He, Amentoflavone suppresses tumor growth in ovarian cancer by modulating Skp2, Life Sci. 189 (2017) 96–105.
[37] C. Li, L. Yu, H. Xue, Z. Yang, Y. Yin, B. Zhang, M. Chen, H. Ma, Nuclear AMPK regulated CARM1 stabilization impacts autophagy in aged heart, Biochem. Biophys. Res. Commun. 486 (2017) 398–405.
[38] W. Ge, R. Guo, J. Ren, AMP-dependent kinase and autophagic flux are involved in aldehyde dehydrogenase-2-induced protection against cardiac toxicity of ethanol, Free Radic. Biol. Med. 51 (2011) 1736–1748.
[39] E.J. Miller, J. Li, L. Leng, C. McDonald, T. Atsumi, R. Bucala, L.H. Young, Macrophage migration inhibitory factor stimulates AMP-activated protein kinase in the ischaemic heart, Nature 451 (2008) 578–582.
[40] C.D. Spies, M. Sander, K. Stangl, J. Fernandez-Sola, V.R. Preedy, E. Rubin,

S. Andreasson, E.Z. Hanna, W.J. Kox, Effects of alcohol on the heart, Curr. Opin. Crit. Care 7 (2001) 337–343.
[41] J. Ren, L.E. Wold, Mechanisms of alcoholic heart disease, Ther. Adv. Cardiovasc. Dis. 2 (2008) 497–506.
[42] Y. Zhang, A.T. Whaley-Connell, J.R. Sowers, J. Ren, Autophagy as an emerging target in cardiorenal metabolic disease: from pathophysiology to management, Pharmacol. Ther. 191 (2018) 1–22.
[43] Z. Li, J. Huang, H. Yuan, Z. Chen, Q. Luo, S. Lu, SIRT2 inhibits non-small cell lung cancer cell growth through impairing Skp2-mediated p27 degradation, Oncotarget 7 (2016) 18927–18939.
[44] S. Wei, P.C. Chu, H.C. Chuang, W.C. Hung, S.K. Kulp, C.S. Chen, Targeting the oncogenic E3 ligase Skp2 in prostate and breast cancer cells with a novel energy restriction-mimetic agent, PLoS One 7 (2012) e47298.